

Omnidirectional Transfer for Quasilinear Lifelong Learning

Joshua T. Vogelstein^{1†,*}, Jayanta Dey^{1,†}, Hayden S. Helm^{1,†}, Will LeVine¹, Ronak D. Mehta¹, Ali Geisa¹, Gido M. van de Ven^{3,4}, Emily Chang¹, Chenyu Gao¹, Weiwei Yang², Bryan Tower², Jonathan Larson², Christopher M. White², and Carey E. Priebe¹

Abstract. In biological learning, data are used to improve performance not only on the current task, but also on previously encountered and as yet unencountered tasks. In contrast, classical machine learning starts from a blank slate, or *tabula rasa*, using data only for the single task at hand. While typical transfer learning algorithms can improve performance on future tasks, their performance on prior tasks degrades upon learning new tasks (called catastrophic forgetting). Many recent approaches for continual or lifelong learning have attempted to *maintain* performance given new tasks. But striving to avoid forgetting sets the goal unnecessarily low: the goal of lifelong learning, whether biological or artificial, should be to *improve* performance on all tasks (including past and future) with any new data. We propose omnidirectional transfer learning algorithms, which includes two special cases of interest: decision forests and deep networks. Our key insight is the development of the *omni-voter* layer, which ensembles representations learned independently on all tasks to jointly decide how to proceed on any given new data point, thereby improving performance on both past and future tasks. Our algorithms demonstrate omnidirectional transfer in a variety of simulated and real data scenarios, including tabular data, image data, spoken data, and adversarial tasks. Moreover, they do so with quasilinear space and time complexity.

1 Introduction Learning is the process by which an intelligent system improves performance on a given task by leveraging data [1]. In biological learning, learning is lifelong, with agents continually building on past knowledge and experiences, improving on many tasks given data associated with any task. For example, learning a second language often improves performance in an individual’s native language [2]. In classical machine learning, the system often starts with essentially zero knowledge, a “tabula rasa”, and is optimized for a single task [3, 4]. While it is relatively easy to *simultaneously* optimize for multiple tasks (multi-task learning) [5], it has proven much more difficult to *sequentially* optimize for multiple tasks [6, 7]. Specifically, classical machine learning systems, and natural extensions thereof, exhibit “catastrophic forgetting” when trained sequentially, meaning their performance on the prior tasks drops precipitously upon training on new tasks [8, 9]. This is in contrast to many biological learning settings, such as the second language learning setting mentioned above.

In the past 30 years, a number of sequential task learning algorithms have attempted to overcome catastrophic forgetting. These approaches naturally fall into one of two camps. In one, the algorithm has fixed resources, and so must reallocate resources (essentially compressing representations) in order to incorporate new knowledge [10–14]. Biologically, this corresponds to adulthood, where brains have a nearly fixed or decreasing number of cells and synapses. In the other, the algorithm adds (or builds) resources as new data arrive [15–17]. Biologically, this corresponds to development, where brains grow by adding cells, synapses, etc.

Approaches from both camps demonstrate some degree of continual (or lifelong) learning [18]. In particular, they can sometimes learn new tasks while not catastrophically forgetting old tasks. However, as we will show, many state of the art lifelong learning algorithms are unable to transfer knowledge forward, and none are able to transfer knowledge backward with small sample sizes where it is particularly important. This inability to omnidirectionally transfer has been identified as one of the key

¹Johns Hopkins University (JHU), ²Microsoft Research, ³Baylor College of Medicine, ⁴University of Cambridge

† denotes equal contribution, * corresponding author: jovo@jhu.edu

obstacles limiting the capabilities of artificial intelligence [19, 20].

We present an approach to lifelong learning called “omnidirectional learning”. Omnidirectional learning algorithms build on the ideas introduced in Progressive Neural Networks (ProgNN) [16], in which new tasks yield additional representational capacity. However, although ProgNN’s are able to transfer forwards, they fail to transfer backwards. Moreover, as we will show, ProgNN requires quadratic space and time complexity in sample size. Our key innovation is the introduction of representation ensembling which enables omnidirectional transfer via an “omni-voter” layer, reducing computational time and space from quadratic to quasilinear (i.e., linear up to polylog terms).

We implement two complementary omnidirectional learning algorithms, one based on decision forests (Omnidirectional Forests, ODIF), and another based on deep networks (Omnidirectional Networks, ODIN). Both ODIF and ODIN demonstrate forward and backward transfer, while maintaining computational efficiency. Simulations illustrate their learning capabilities, including performance properties in the presence of adversarial tasks. We then demonstrate their learning capabilities in vision and language benchmark applications. Although the omnidirectional algorithms presented here are primarily resource building, we illustrate that they can effectively leverage prior representations. This ability implies that the algorithm can convert from a “juvenile” resource building state to the “adult” resource recruiting state – all while maintaining key omnidirectional learning capabilities and efficiencies.

2 Background

2.1 Classical Machine Learning Classical supervised learning [21] considers random variables $(X, Y) \sim P_{X,Y}$, where X is an \mathcal{X} -valued input, Y is a \mathcal{Y} -valued label (or response), and $P_{X,Y} \in \mathcal{P}_{X,Y}$ is the joint distribution of (X, Y) . Given a loss function $\ell : \mathcal{Y} \times \mathcal{Y} \rightarrow [0, \infty)$, the goal is to find the hypothesis (also called predictor or decision rule), $h : \mathcal{X} \rightarrow \mathcal{Y}$ that minimizes expected loss, or *risk*, $R(h) = \mathbb{E}_{X,Y} [\ell(h(X), Y)]$. A learning algorithm (or rule) is a function f that maps data sets (n training samples) to a hypothesis, where a data set $\mathbf{S}_n = \{X_i, Y_i\}_{i=1}^n$ is a set of n input/response pairs. Assume n samples of (X, Y) pairs are independently and identically distributed from some true but unknown $P_{X,Y}$ [21]. A learning algorithm is evaluated on its generalization error (or expected risk): $\mathbb{E}[R(f(\mathbf{S}_n))]$, where the expectation is taken with respect to the true but unknown distribution governing the data, $P_{X,Y}$. The goal is to choose a learner f that learns a hypothesis h that has a small generalization error for the given task [22].

2.2 Lifelong Learning Lifelong learning generalizes classical machine learning in a few ways: (i) instead of one task, there is an environment \mathcal{T} of (possibly infinitely) many tasks, (ii) data arrive sequentially, rather than in batch mode, and (iii) there are computational complexity constraints on the learning algorithm and hypotheses. This third requirement is crucial, though often implicit. Consider, for example, the algorithm that stores all the data, and then retrains everything from scratch each time a new sample arrives. Without computational constraints, such an algorithm could be classified as a lifelong learner; we do not think such a label is appropriate for that algorithm.

The goal in lifelong learning therefore is, given new data and a new task, use all the existing data to achieve lower generalization error on this new task, while also using the new data to obtain a lower generalization error on the previous tasks. This is distinct from classical online learning scenarios, because the previously experienced tasks may recur, so we are concerned about maintaining and improving performance on those tasks as well. Previous work in lifelong learning falls loosely into two algorithmic camps: (i) continually updating a fixed parametric model as new tasks arrive, and (ii) adding resources as new tasks arrive. Some approaches additionally store or replay previously encountered data to reduce forgetting [23–25]. In ‘task-aware’ scenarios, the learner is aware of all task details for

all tasks, meaning that the hypotheses are of the form $h : \mathcal{X} \times \mathcal{T} \rightarrow \mathcal{Y}$. In ‘task-unaware’ (or task agnostic [26]) scenarios the learner may not know that the task has changed at all, which means that the hypotheses are of the form, $h : \mathcal{X} \rightarrow \mathcal{Y}$. We only address task-aware scenarios here.

2.3 Reference algorithms We compared our approaches to nine reference lifelong learning methods. These algorithms can be classified into two groups based on whether they build new resources, or leverage fixed resources, given new tasks. Among them, Progressive Neural Networks (ProgNN) [16] and Deconvolution-Factorized CNNs (DF-CNN) [17] learn new tasks by building new resources. For ProgNN, for each new task a new ‘column’ of network is introduced. In addition to introducing this column, lateral connections from all previous columns to the new column are added. These lateral connections are computationally costly, as explained below. DF-CNN [17] is a lifelong learning algorithm that improves upon ProgNN by introducing a knowledge base with lateral connections to each new column, thereby avoiding all pairwise connections, and dramatically reducing computational costs.

The other seven algorithms, Elastic Weight Consolidation (EWC) [10], Online-EWC (O-EWC) [13], Synaptic Intelligence (SI) [11], Learning without Forgetting (LwF) [12], ‘None’ and two variants of exact replay (Total Replay and Partial Replay) [27], all have fixed capacity resources. For the first variant of exact replay, referred to as “Total replay”, we replay all the data from all previous tasks whenever a new task is encountered. In the lifelong learning literature this is typically called “offline training”. Replaying everything might however not be needed [25], and for the second variant of exact replay the amount of replay for each new task is fixed to the number of training samples in the new task, and the samples to be replayed are randomly selected from all the data of the previous tasks. For the baseline ‘None’, the network was incrementally trained on all tasks in the standard way while always only using the data from the current task. The implementations for all of the algorithms are adapted from open source codes [17, 28]; for implementation details, see Appendix C.3.

3 Evaluation Criteria Others have previously introduced criteria to evaluate transfer, including forward and backward transfer [29, 30]. These definitions typically compare the difference, rather than the ratio, between learning with and without transfer. Pearl [19] introduced the transfer benefit ratio, which builds directly off relative efficiency from classical statistics [22]. Our definitions are closely related to his. *Transfer efficiency* is the ratio of the generalization error of (i) an algorithm that has learned only from data associated with a given task, to (ii) the same learning algorithm that also has access to other data. Let R^t be the risk associated with task t , and \mathbf{S}_n^t be the data from \mathbf{S}_n that is specifically associated with task t , so $R^t(f(\mathbf{S}_n^t))$ is the risk on task t of the hypothesis learned by f only on task t data, and $R^t(f(\mathbf{S}_n))$ denotes the risk on task t of the hypothesis learned on all the data.

Definition 1 (Transfer Efficiency). *The transfer efficiency of algorithm f for given task t with sample size n is $\text{TE}_n^t(f) := \mathbb{E} [R^t(f(\mathbf{S}_n^t))] / \mathbb{E} [R^t(f(\mathbf{S}_n))]$. We say that algorithm f has transfer learned for task t with data \mathbf{S}_n if and only if $\text{TE}_n^t(f) > 1$.*

To evaluate a lifelong learning algorithm while respecting the streaming nature of the tasks, it is convenient to consider two extensions of transfer efficiency. *Forward* transfer efficiency is the expected ratio of the risk of the learning algorithm with (i) access only to task t data, to (ii) access to the data up to and including the last observation from task t . This quantity measures the relative effect of previously seen out-of-task data on the performance on task t . Formally, let $N^t = \max\{i : T_i = t\}$, be the index of the last occurrence of task t in the data sequence. Let $\mathbf{S}_n^{\leq t} = \{(X_1, Y_1, T_1), \dots, (X_{N^t}, Y_{N^t}, T_{N^t})\}$ be all data up to and including that data point.

Definition 2 (Forward Transfer Efficiency). *The forward transfer efficiency of f for task t given n*

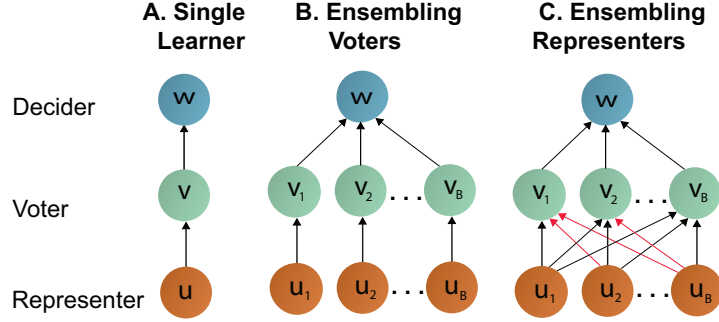


Figure 1: Schemas of composable hypotheses. Ensembling voters is a well-established practice, including random forests and gradient boosted trees. Ensembling representations was previously used in lifelong learning scenarios, but without connections from future tasks to past ones. We introduce such connections, thereby enabling backward transfer.

samples is $\text{FTE}_n^t(f) := \mathbb{E} [R^t (f(\mathbf{S}_n^t))] / \mathbb{E} [R^t (f(\mathbf{S}_n^{<t}))]$.

We say an algorithm (positive) forward transfers for task t if and only if $\text{FTE}_n^t(f) > 1$. In other words, if $\text{FTE}_n^t(f) > 1$, then the algorithm has used data associated with past tasks to improve performance on task t .

One can also determine the rate of *backward* transfer by comparing $R^t (f(\mathbf{S}_n^{<t}))$ to the risk of the hypothesis learned having seen the entire training dataset. More formally, backward transfer efficiency is the expected ratio of the risk of the learned hypothesis with (i) access to the data up to and including the last observation from task t , to (ii) access to the entire dataset. Thus, this quantity measures the relative effect of future task data on the performance on task t .

Definition 3 (Backward Transfer Efficiency). *The backward transfer efficiency of f for task t given n samples is $\text{BTE}_n^t(f) := \mathbb{E} [R^t (f(\mathbf{S}_n^{<t}))] / \mathbb{E} [R^t (f(\mathbf{S}_n))]$.*

We say an algorithm (positive) backward transfers for task t if and only if $\text{BTE}_n^t(f) > 1$. In other words, if $\text{BTE}_n^t(f) > 1$, then the algorithm has used data associated with future tasks to improve performance on previous tasks.

After observing m tasks, the extent to which the TE for the j^{th} task comes from forward transfer versus from backwards transfer depends on the order of the tasks. If we have a sequence in which tasks do not repeat, transfer efficiency for the first task is all backwards transfer, for the last task it is all forwards transfer, and for the middle tasks it is a combination of the two. In general, TE factorizes into FTE and BTE:

$$\text{TE}_n^t(f) = \frac{\mathbb{E} [R^t (f(\mathbf{S}_n^t))]}{\mathbb{E} [R^t (f(\mathbf{S}_n))]} = \frac{\mathbb{E} [R^t (f(\mathbf{S}_n^t))]}{\mathbb{E} [R^t (f(\mathbf{S}_n^{<t}))]} \times \frac{\mathbb{E} [R^t (f(\mathbf{S}_n^{<t}))]}{\mathbb{E} [R^t (f(\mathbf{S}_n))]}.$$

Throughout, we will report log TE so that positive transfer corresponds to $\text{TE} > 1$.

4 Omnidirectional Algorithms Our approach to lifelong learning relies on hypotheses that can be decomposed into three constituent parts: $h(\cdot) = w \circ v \circ u(\cdot)$ (Figure 1A). The representer, $u : \mathcal{X} \mapsto \tilde{\mathcal{X}}$, maps an \mathcal{X} -valued input into an internal representation space $\tilde{\mathcal{X}}$ [31, 32]. The voter $v : \tilde{\mathcal{X}} \mapsto \Delta_{\mathcal{Y}}$ maps the transformed data into a posterior distribution (or, more generally, a score) on the response space \mathcal{Y} . Finally, a decider $w : \Delta_{\mathcal{Y}} \mapsto \mathcal{Y}$, produces a predicted label.¹ See Appendix A for a concrete example

¹In coding theory, these three functions are frequently called the encoder, channel, and decoder, respectively [33, 34]

using a decision tree.

One can generalize the above decomposition by allowing for multiple representers. Given B different representers, one can attach a single voter to each representer, yielding B different voters (Figure 1B). Doing so requires generalizing the definition of a decider, which would operate on multiple voters. The decider is then said to *ensemble the voters*. This is the learning paradigm behind boosting [35] and bagging [36]—indeed, decision forests are a canonical example of a decision function operating on a collection of B outputs [37]. A decision forest learns B different decision trees, each of which has a tree structure corresponding to a representer. Each tree is assigned a voter that outputs that single tree’s guess as to probability that an observation is in any class. The decider outputs the most likely class averaged over the trees.

A further generalization of the above decomposition allows for *each voter to ensemble the representers* (Figure 1C). Doing so requires the introduction of an *omni-voter* layer, which is formally distinct from the voter function described above that operates solely on a single representer. The omni-voter ensembles all the existing representations, regardless of the order in which they were learned. In this scenario, like with bagging and boosting, the ensemble of voters then feeds into the single decider. When each representer has learned complementary representations, this latter approach has certain appealing properties, particularly in multiple task scenarios, including lifelong learning. See Appendix B for a concrete example. We developed two different omnidirectional learning algorithms that ensemble representations (see Appendix C for full details, including pseudocode). Omnidirectional Forest (ODIF) uses decision forests as the representers, specifically a variant of decision forests called ‘Uncertainty Forest’ [38]. An Omnidirectional Network (ODIN) uses deep networks as the representers. In either case, as new data from a new task arrives, our algorithms first build a new independent representer (using forests or networks). Then, it builds the voter for this new task, which intergrates information across all existing representers, thereby enabling forward transfer. If new data arrive from an old task, it can leverage the new representers to update the voters from the old tasks, thereby enabling backward transfer. In either case, new test data are passed through all existing representers and corresponding voters to make a prediction.

ODIN was motivated by ProgNN, but differs from ProgNN in two key ways. First, recall that ProgNN builds a new neural network ‘column’ for each new task, and also builds lateral connections between the new column, and all previous columns. In contrast, ODIN excludes those lateral connections, thereby greatly reducing the number of parameters and train time. Moreover, this makes each representation independent, thereby potentially avoiding interference across representations. Second, for inference on task j data, assuming we have observed tasks up to $J > j$, ProgNN only leverages representations learned from tasks up to j , thereby excluding tasks $j + 1, \dots, J$. In contrast, ODIN leverages representations from all J tasks. This difference enables backward transfer. ODIF adds yet another difference by replacing the deep network representers with random forest representers. This has the effect of making the capacity, space and time complexity scale with the complexity and sample size of each task. In contrast, both ProgNN and ODIN have a fixed capacity for each task, even if the tasks have very different sample sizes and complexities.

5 Results

5.1 A computational taxonomy of lifelong learning Lifelong learning approaches can be divided into those with fixed resources, and those with growing resources. We therefore quantify the computational space and time complexity of the internal representation of a number of algorithms, using both theoretical analysis and empirical investigations. We also study the representation capacity of these

Table 1: Capacity, space, and time constraints of various lifelong learning algorithms. We show soft-O notation ($\tilde{O}(\cdot, \cdot)$ defined in main text) as a function of n and T , as well as the common setting where n is proportional to T . Our omnidirectional algorithms are the only algorithms whose representation space grows, but sub-quadratically with n or T , and **ODIF** is the only algorithm whose time complexity is linear in n for learning the representation.

Parametric	Capacity	Space		Time		Examples
	(n, T)	(n, T)	$(n \propto T)$	(n, T)	$(n \propto T)$	
parametric	1	T	n	nT	n^2	EWC
parametric	1	1	1	n	n	O-EWC, SI, LwF
parametric	1	n	n	nT	n^2	Total Replay
semiparametric	T	T^2	n^2	nT	n^2	ProgNN
semiparametric	T	T	n	n	n	DF-CNN
semiparametric	T	$T + n$	n	n	n	ODIN
nonparametric	n	n	n	n	n	ODIF

algorithms. We use the soft-O notation \tilde{O} to quantify complexity [39]. Letting n be the sample size and T be the number of tasks, we write that a lifelong learning algorithm is $f(n, t) = \tilde{O}(g(n, T))$ when $|f|$ is bounded above asymptotically by a function g of n and T up to a constant factor and polylogarithmic terms. Table 1 summarizes the capacity, space and time complexity of several reference algorithms, as well as our **ODIN** and **ODIF**. For the deep learning methods, we assume that the number of iterations is proportional to the number of samples. For space and time complexity, the table shows results as a function of n and T , as well as the common scenario where sample size per task is fixed and therefore proportional to the number of tasks, $n \propto T$.

Fixed resource lifelong learning methods are parametric, in that the representational capacity is invariant to sample size and task number, have computational space complexity of $\tilde{O}(1)$ [22]. Given a sufficiently large number of tasks, without placing constraints on the relationship between the tasks, eventually all parametric methods will catastrophically forget at least some things. EWC, Online EWC, SI, and LwF are all examples of parametric lifelong learning algorithms.

Semi-parametric algorithms are algorithms whose representational capacity grows slower than sample size. For example, if T is increasing slower than n (e.g., $T \propto \log n$), then algorithms whose capacity is proportional to T are semi-parametric. ProgNN is semi-parametric with space complexity $\tilde{O}(T^2)$ due to the lateral connections. Moreover, the time complexity for ProgNN also scales quadratically with n when $n \propto T$. Thus, an algorithm that literally stores all the data it has ever seen, and retrain a fixed size network on all that data with the arrival of each new task, would have smaller space complexity and the same time complexity as ProgNN. For comparison, we implement such an algorithm and refer to it as Total Replay. DF-CNN improves upon ProgNN by introducing a knowledge base with lateral connections to each new column, thereby avoiding all pairwise connections. Because these semi-parametric methods have a fixed representational capacity per task, they will either lack the representation capacity to perform well given sufficiently complex tasks, and/or will waste resources for very simple tasks.

ODIN eliminates the lateral connections between columns of the network, thereby reducing space complexity down to $\tilde{O}(T)$. **ODIN** stores all the data to enable backwards transfer, but retains linear time complexity. **ODIF** is the only non-parametric lifelong learning algorithm to our knowledge. Its capacity, space and time complexity are all $\tilde{O}(n)$, meaning that its representational capacity naturally increases with the complexity of each task.

5.2 Illustrating Omnidirectional Learning with ODIF

Omnidirectional learning in a simple environment Consider a very simple two-task environment: Gaussian XOR and Gaussian Exclusive NOR (XNOR) (Figure 2A, see Appendix D for details). The two tasks share the exact same discriminant boundaries: the coordinate axes. Thus, transferring from one task to the other merely requires learning a bit flip. We sample 750 samples from XOR, followed by another 750 samples from XNOR.

ODIF and random forests (RF) achieve the same generalization error on XOR when training with XOR data (Figure 2Bi). But because RF does not account for a change in task, when XNOR data appear, RF performance on XOR gets worse and worse. In contrast, ODIF continues to improve on XOR given XNOR data, demonstrating backwards transfer. Now consider the generalization error on XNOR (Figure 2Bii). Both ODIF and RF are at chance levels when only XOR data are available. When XNOR data are available, RF must unlearn everything it learned from the XOR data, and thus its performance on XNOR starts out nearly maximally inaccurate, and quickly improves. On the other hand, because ODIF can leverage the representer learned using the XOR data, upon getting *any* XNOR data, it immediately performs quite well, and then continues to improve with further XNOR data, demonstrating forward transfer (Figure 2Biii). ODIF demonstrates positive forward and backward transfer for all sample sizes, whereas RF fails to demonstrate forward or backward transfer, and eventually catastrophically forgets the previous tasks.

Omnidirectional learning in adversarial environments Statistics has a rich history of *robust learning* [40], and machine learning has recently focused on *adversarial learning* [41]. However, in both cases the focus is on adversarial *examples*, rather than adversarial *tasks*. In the context of omnidirectional learning, we informally define a task t to be adversarial with respect to task t' if the true joint distribution of task t , without any domain adaptation, impedes performance on task t' . In other words, training data from task t can only add noise, rather than signal, for task t' . An adversarial task for Gaussian XOR is Gaussian XOR rotated by 45° (R-XOR) (Figure 2Aiii). Training on R-XOR therefore impedes the performance of ODIF on XOR, and thus backward transfer falls below one, demonstrating graceful forgetting (Figure 2Ci). Because R-XOR is more difficult than XOR for ODIF (because the discriminant boundaries are oblique [42]), and because the discriminant boundaries are learned imperfectly with finite data, data from XOR can actually improve performance on R-XOR, and thus forward transfer is positive. In contrast, both forward and backward transfer are negative for RF.

To further investigate this relationship, we designed a suite of R-XOR examples, varying the rotation angle θ between 0° and 360° , sampling 100 points from XOR, and another 100 from each R-XOR (Figure 2Cii). As the angle increases from 0° to 45° , log BTE flips from positive (≈ 0.30) to negative (≈ -0.06). The 45° -XOR is the maximally adversarial R-XOR. Thus, as the angle further increases, log BTE increases back up to ≈ 0.30 at 90° , which has an identical discriminant boundary to XOR. Moreover, when θ is fixed at 25° , BTE monotonically increases with sample size (Figure 2Ciii).

Together, these experiments indicate that the amount of transfer can be a complicated function of (i) the difficulty of learning good representations for each task, (ii) the relationship between the two tasks, and (iii) the sample size of each. Appendix D further investigates this phenomenon in a multi-spiral environment.

5.3 Real data experiments We consider two modalities for real data experiments: vision and language. Below we provide a detailed analysis of the performance of lifelong learning algorithms in vision data; Appendix E provides details for our language experiments, which have qualitatively similar results illustrating that ODIF is a modality agnostic, sample and computationally efficient, lifelong learning

algorithm.

The CIFAR 100 challenge [43], consists of 50,000 training and 10,000 test samples, each a 32x32 RGB image of a common object, from one of 100 possible classes, such as apples and bicycles. CIFAR 10x10 divides these data into 10 tasks, each with 10 classes [17] (see Appendix E for details). We compare \mathcal{O}_{DIF} and \mathcal{O}_{DIN} to the deep lifelong learning algorithms discussed above. The below experiments use only 500 training samples per task, see Appendix Figure 4 for the corresponding results using 5,000 training samples per task.

Resource Growing Experiments We first compare \mathcal{O}_{DIF} and \mathcal{O}_{DIN} to state-of-the-art resource growing algorithms: ProgNN and DF-CNN (Figure 3, top panels). Both \mathcal{O}_{DIF} and \mathcal{O}_{DIN} demonstrate positive forward transfer for every task (\mathcal{O}_{DIF} increases nearly monotonically), indicating they are robust to distributional shift in ways that ProgNN and DF-CNN are not. \mathcal{O}_{DIN} and \mathcal{O}_{DIF} uniquely demonstrate positive backwards transfer, \mathcal{O}_{DIN} is actually monotonically increasing, indicating that with each new task, performance on all prior tasks increases (and \mathcal{O}_{DIF} nearly monotonically increases BTE as well). In contrast, while neither ProgNN nor DF-CNN exhibit catastrophic forgetting, they also do not exhibit any positive backward transfer. Final transfer efficiency per task is the transfer efficiency associated with that task having seen all the data. \mathcal{O}_{DIF} and \mathcal{O}_{DIN} both demonstrate positive final transfer efficiency for all tasks, whereas ProgNN and DF-CNN both exhibit negative final transfer efficiency for at least one task.

Resource Constrained Experiments It is possible that the above algorithms are leveraging additional resources to improve performance without meaningfully transferring information between representations. To address this concern, we devised a ‘resource constrained’ variant of \mathcal{O}_{DIF} . In this constrained variant, we compare the lifelong learning algorithm to its single task variant, but ensure that they both have the same amount of resources. For example, on Task 2, we would compare \mathcal{O}_{DIF} with 20 trees (10 trained on 500 samples from Task 1, and another 10 trained on 500 samples from Task 2) to RF with 20 trees (all trained on 500 samples Task 2). If \mathcal{O}_{DIF} is able to meaningfully transfer information across tasks, then its resource-constrained FTE and BTE will still be positive. Indeed, FTE remains positive after enough tasks, and BTE is actually invariant to this change (Figure 3, bottom left and center). In contrast, all of the reference algorithms that have fixed resources exhibit negative forward and backward transfer. Moreover, the reference algorithms also all exhibit negative final transfer efficiency on each task, whereas our resource constrained \mathcal{O}_{DIF} maintains positive final transfer on every task (Figure 3, top right). Interestingly, when using 5,000 samples per task, replay methods are able to demonstrate positive forward and backwards transfer (Supplementary Figure 4), although they require quadratic time. Note that in this experiment, building the single task learners actually required substantially *more* resources, specifically, $10 + 20 + \dots + 100 = 550$ trees, as compared with only 100 trees in the prior experiments. In general, to ensure single task learners use the same amount of resources per task as omnidirectional learners requires $\tilde{O}(n^2)$ resources, where as \mathcal{O}_{DIF} only requires $\tilde{O}(n)$, a polynomial reduction in resources.

Resource Recruiting Experiments The binary distinction we made above, algorithms either build resources or reallocate them, is a false dichotomy, and biologically unnatural. In biological learning, systems develop from building (juvenile) to recruiting (adult) resources. We therefore trained \mathcal{O}_{DIF} on the first nine CIFAR 10x10 tasks using 50 trees per task, with 500 samples per task. For the tenth task, we could (i) select the 50 trees (out of the 450 existing trees) that perform best on task 10 (recruiting), (ii) train 50 new trees, as \mathcal{O}_{DIF} would normally do (building), (iii) build 25 and recruit 25 trees (hybrid), or (iv) ignore all prior trees (RF). \mathcal{O}_{DIF} outperforms other approaches except when 5,000 training samples

are available, but the recruiting approach is nearly as good as `ODIF` (Figure 3, bottom right). This result motivates future work to investigate optimal strategies for determining how to optimally leverage existing resources given a new task, and task-unaware settings.

Adversarial Experiments Consider the same CIFAR 10x10 experiment above, but, for tasks two through nine, randomly permute the class labels within each task, rendering each of those tasks adversarial with regard to the first task (because the labels are uninformative). Figure 4A indicates that backward transfer efficiency for both `ODIF` and `ODIN` is invariant to such label shuffling (the other algorithms also seem invariant to label shuffling, but did not demonstrate positive backwards transfer). Now, consider a Rotated CIFAR experiment, which uses only data from the first task, divided into two equally sized subsets (making two tasks), where the second subset is rotated by different amounts (Figure 4, right). Transfer efficiency of both `ODIF` and `ODIN` is nearly invariant to rotation angle, whereas the other approaches are far more sensitive to rotation angle. Note that zero rotation angle corresponds to the two tasks *having identical distributions*.

6 Discussion We introduced quasilinear representation ensembling as an approach to omnidirectional lifelong learning. The two specific algorithms we developed, `ODIF` and `ODIN`, demonstrate the possibility of achieving both forward and backward transfer, due to leveraging resources (representers) learned for other tasks without undue computational burdens. Forest-based representation ensembling approaches can easily add new resources when appropriate. This work further therefore motivates additional work on deep learning to enable dynamically adding resources when appropriate [44].

To achieve backward transfer, `ODIF` and `ODIN` stored old data to vote on the newly learned transformers. Because the representation space scales quasilinearly with sample size, storing the data does not increase the computational complexity of the algorithm, and it remains quasilinear. In contrast, ProgNN has representation space scaling quadratically with sample size, rendering it less computationally efficient than merely storing all the data and retraining (which ‘Total Replay’ does). Both ProgNN and Total Replay, however, have quadratic time complexity, unlike `ODIF` and `ODIN`. Nonetheless, a natural extension of this work would obviate the need to store any data.

While we employed representation ensembling to address catastrophic forgetting, the paradigm of ensembling *representations* rather than *learners* can be readily applied more generally. For example, ‘batch effects’ (sources of variability unrelated to the scientific question of interest) have plagued many fields of inquiry, including neuroscience [45] and genomics [46]. Similarly, federated learning is becoming increasingly central in artificial intelligence, due to its importance in differential privacy [47]. This may be particularly important in light of global pandemics such as COVID-19, where combining small datasets across hospital systems could enable more rapid discoveries [48].

Finally, biological learning leverages ensembles of representations, so we hope this work motivates a tighter connection between biological and machine learning. By carefully designing experiments in which both behaviors and brain are observed while learning across sequences of tasks (possibly in multiple stages of neural development or degeneration), we may be able to learn more about how biological agents are able to omnidirectionally learn so efficiently, and transfer that understanding to building more effective artificial intelligences. In the meantime, our code, including code to reproduce the experiments in this manuscript, is available from <http://proglearn.neurodata.io/>.

Acknowledgements The authors thank the support of the NSF-Simons Research Collaborations on the Mathematical and Scientific Foundations of Deep Learning (NSSF grant 2031985). We also thank Raman Arora, Dinesh Jayaraman, Rene Vidal, Jeremias Sulam, Guillermo Sapiro, and Michael Powell for helpful discussions. This work is graciously supported by the Defense Advanced Research

Projects Agency (DARPA) Lifelong Learning Machines program through contracts FA8650-18-2-7834 and HR0011-18-2-0025. Research was partially supported by funding from Microsoft Research and the Kavli Neuroscience Discovery Institute.

References

- [1] Tom M Mitchell. Machine learning and data mining. Communications of the ACM, 42(11):30–36, 1999.
- [2] Jing Zhao, Blanca Quiroz, L Quentin Dixon, and R Malatesha Joshi. Comparing Bilingual to Monolingual Learners on English Spelling: A Meta-analytic Review. Dyslexia, 22(3):193–213, August 2016.
- [3] V Vapnik and A Chervonenkis. On the Uniform Convergence of Relative Frequencies of Events to Their Probabilities. Theory Probab. Appl., 16(2):264–280, January 1971.
- [4] L G Valiant. A Theory of the Learnable. Commun. ACM, 27(11):1134–1142, November 1984. URL <http://doi.acm.org/10.1145/1968.1972>.
- [5] Rich Caruana. Multitask learning. Machine learning, 28(1):41–75, 1997.
- [6] Sebastian Thrun. Is learning the n-th thing any easier than learning the first? In Advances in neural information processing systems, pages 640–646, 1996.
- [7] Sebastian Thrun and Lorien Pratt. Learning to Learn. Springer Science & Business Media, December 2012. URL https://market.android.com/details?id=book-X_jpBwAAQBAJ.
- [8] Michael McCloskey and Neal J Cohen. Catastrophic interference in connectionist networks: The sequential learning problem. In Psychology of learning and motivation, volume 24, pages 109–165. Elsevier, 1989.
- [9] James L McClelland, Bruce L McNaughton, and Randall C O’Reilly. Why there are complementary learning systems in the hippocampus and neocortex: insights from the successes and failures of connectionist models of learning and memory. Psychological review, 102(3):419, 1995.
- [10] James Kirkpatrick, Razvan Pascanu, Neil Rabinowitz, Joel Veness, Guillaume Desjardins, Andrei A Rusu, Kieran Milan, John Quan, Tiago Ramalho, Agnieszka Grabska-Barwinska, Demis Hassabis, Claudia Clopath, Dharshan Kumaran, and Raia Hadsell. Overcoming catastrophic forgetting in neural networks. Proceedings of the national academy of sciences, 114(13):3521–3526, 2017.
- [11] Friedemann Zenke, Ben Poole, and Surya Ganguli. Continual learning through synaptic intelligence. In Proceedings of the 34th International Conference on Machine Learning-Volume 70, pages 3987–3995. JMLR. org, 2017.
- [12] Zhizhong Li and Derek Hoiem. Learning without forgetting. IEEE transactions on pattern analysis and machine intelligence, 40(12):2935–2947, 2017.
- [13] Jonathan Schwarz, Jelena Luketina, Wojciech M Czarnecki, Agnieszka Grabska-Barwinska, Yee Whye Teh, Razvan Pascanu, and Raia Hadsell. Progress & compress: A scalable framework for continual learning. arXiv preprint arXiv:1805.06370, 2018.
- [14] Chelsea Finn, Aravind Rajeswaran, Sham Kakade, and Sergey Levine. Online meta-learning. In Kamalika Chaudhuri and Ruslan Salakhutdinov, editors, International Conference on Machine Learning, volume 97 of Proceedings of Machine Learning Research, pages 1920–1930, Long Beach, California, USA, 06 2019. PMLR. URL <http://proceedings.mlr.press/v97/finn19a.html>.
- [15] Paul Ruvolo and Eric Eaton. ELLA: An Efficient Lifelong Learning Algorithm. In International Conference on Machine Learning, volume 28, pages 507–515, February 2013. URL <http://proceedings.mlr.press/v28/ruvolo13.html>.
- [16] Andrei A Rusu, Neil C Rabinowitz, Guillaume Desjardins, Hubert Soyer, James Kirkpatrick, Koray

- Kavukcuoglu, Razvan Pascanu, and Raia Hadsell. Progressive neural networks. arXiv preprint arXiv:1606.04671, 2016.
- [17] Seungwon Lee, James Stokes, and Eric Eaton. Learning shared knowledge for deep lifelong learning using deconvolutional networks. In Proceedings of the 28th International Joint Conference on Artificial Intelligence, pages 2837–2844, 2019.
- [18] German I Parisi, Ronald Kemker, Jose L Part, Christopher Kanan, and Stefan Wermter. Continual lifelong learning with neural networks: A review. Neural Networks, 2019.
- [19] Judea Pearl. The seven tools of causal inference, with reflections on machine learning. Commun. ACM, February 2019.
- [20] Gary Marcus and Ernest Davis. Rebooting AI: Building Artificial Intelligence We Can Trust. Pantheon, September 2019.
- [21] Mehryar Mohri, Afshin Rostamizadeh, and Ameet Talwalkar. Foundations of Machine Learning. MIT Press, November 2018. URL <https://market.android.com/details?id=book-dWB9DwAAQBAJ>.
- [22] Peter J Bickel and Kjell A Doksum. Mathematical statistics: basic ideas and selected topics, volumes I-II package. Chapman and Hall/CRC, 2015.
- [23] Anthony Robins. Catastrophic forgetting, rehearsal and pseudorehearsal. Connection Science, 7(2):123–146, 1995.
- [24] Hanul Shin, Jung Kwon Lee, Jaehong Kim, and Jiwon Kim. Continual learning with deep generative replay. In Advances in Neural Information Processing Systems, pages 2990–2999, 2017.
- [25] Gido M van de Ven, Hava T Siegelmann, and Andreas S Tolias. Brain-inspired replay for continual learning with artificial neural networks. Nature communications, 11:4069, 2020.
- [26] Chen Zeno, Itay Golan, Elad Hoffer, and Daniel Soudry. Task Agnostic Continual Learning Using Online Variational Bayes. arXiv, March 2018.
- [27] David Rolnick, Arun Ahuja, Jonathan Schwarz, Timothy Lillicrap, and Gregory Wayne. Experience replay for continual learning. In Advances in Neural Information Processing Systems, pages 350–360, 2019.
- [28] Gido M. van de Ven and Andreas S. Tolias. Three scenarios for continual learning. CoRR, abs/1904.07734, 2019. URL <http://arxiv.org/abs/1904.07734>.
- [29] David Lopez-Paz and Marc’Aurelio Ranzato. Gradient episodic memory for continual learning. In NIPS, 2017.
- [30] Diana Benavides-Prado, Yun Sing Koh, and Patricia Riddle. Measuring Cumulative Gain of Knowledgeable Lifelong Learners. In NeurIPS Continual Learning Workshop, pages 1–8, 2018.
- [31] Ashish Vaswani, Noam Shazeer, Niki Parmar, Jakob Uszkoreit, Llion Jones, Aidan N Gomez, Łukasz Kaiser, and Illia Polosukhin. Attention is All you Need. In I Guyon, U V Luxburg, S Bengio, H Wallach, R Fergus, S Vishwanathan, and R Garnett, editors, Advances in Neural Information Processing Systems 30, pages 5998–6008. Curran Associates, Inc., 2017.
- [32] Jacob Devlin, Ming-Wei Chang, Kenton Lee, and Kristina Toutanova. BERT: pre-training of deep bidirectional transformers for language understanding. CoRR, abs/1810.04805, 2018. URL <http://arxiv.org/abs/1810.04805>.
- [33] Thomas M Cover and Joy A Thomas. Elements of Information Theory. John Wiley & Sons, New York, November 2012.
- [34] Kyunghyun Cho, B van Merriënboer, Caglar Gulcehre, F Bougares, H Schwenk, and Yoshua Bengio. Learning phrase representations using rnn encoder-decoder for statistical machine translation.

- In Conference on Empirical Methods in Natural Language Processing (EMNLP 2014), 2014.
- [35] Yo Freund. Boosting a Weak Learning Algorithm by Majority. Inform. and Comput., 121(2):256–285, September 1995.
 - [36] Leo Breiman. Bagging predictors. Mach. Learn., 24(2):123–140, August 1996.
 - [37] Leo Breiman. Random forests. Machine learning, 45(1):5–32, 2001.
 - [38] Ronak Mehta, Richard Guo, Cencheng Shen, and Joshua Vogelstein. Estimating information-theoretic quantities with random forests. arXiv preprint arXiv:1907.00325, 2019.
 - [39] Iris van Rooij, Mark Blokpoel, Johan Kwisthout, and Todd Wareham. Cognition and Intractability: A Guide to Classical and Parameterized Complexity Analysis. Cambridge University Press, April 2019.
 - [40] Peter J Huber. Robust statistical procedures, volume 68. Siam, 1996.
 - [41] Christian Szegedy, Wojciech Zaremba, Ilya Sutskever, Joan Bruna, Dumitru Erhan, Ian Goodfellow, and Rob Fergus. Intriguing properties of neural networks. In 2nd International Conference on Learning Representations, ICLR 2014, 01 2014.
 - [42] Tyler M Tomita, James Browne, Cencheng Shen, Jaewon Chung, Jesse L Patsolic, Benjamin Falk, Jason Yim, Carey E Priebe, Randal Burns, Mauro Maggioni, and Joshua T Vogelstein. Sparse Projection Oblique Randomer Forests. J. Mach. Learn. Res., 2020.
 - [43] Alex Krizhevsky. Learning multiple layers of features from tiny images. University of Toronto, 05 2012.
 - [44] Jaehong Yoon, Eunho Yang, Jeongtae Lee, and Sung Ju Hwang. Lifelong Learning with Dynamically Expandable Networks. International Conference on Learning Representations, August 2017.
 - [45] E W Bridgeford, S Wang, Z Yang, Z Wang, T Xu, and others. Big Data Reproducibility: Applications in Brain Imaging. bioRxiv, 2020.
 - [46] W Evan Johnson, Cheng Li, and Ariel Rabinovic. Adjusting batch effects in microarray expression data using empirical Bayes methods. Biostatistics, 8(1):118–127, January 2007.
 - [47] Cynthia Dwork. Differential Privacy: A Survey of Results. In Theory and Applications of Models of Computation, pages 1–19. Springer Berlin Heidelberg, 2008.
 - [48] Joshua T Vogelstein, Michael Powell, Allison Koenecke, Ruoxuan Xiong, Nicole Fischer, Sakibul Huq, Adham M Khalafallah, Brian Caffo, Elizabeth A Stuart, Nickolas Papadopoulos, Kenneth W Kinzler, Bert Vogelstein, Shibin Zhou, Chetan Bettgowda, Maximilian F Konig, Brett Mensh, and Susan Athey. Alpha-1 adrenergic receptor antagonists for preventing acute respiratory distress syndrome and death from cytokine storm syndrome. ArXiv, April 2020.
 - [49] Guneet Singh Dhillon, Pratik Chaudhari, Avinash Ravichandran, and Stefano Soatto. A baseline for few-shot image classification. In International Conference on Learning Representations, 2020. URL <https://openreview.net/forum?id=rylXBkrYDS>.
 - [50] Yali Amit and Donald Geman. Shape Quantization and Recognition with Randomized Trees. Neural Comput., 9(7):1545–1588, October 1997.
 - [51] Leo Breiman, Jerome Friedman, Charles J Stone, and Richard A Olshen. Classification and regression trees. CRC press, 1984.
 - [52] M. Denil, D. Matheson, and N. De Freitas. Narrowing the gap: Random forests in theory and in practice. In Eric P. Xing and Tony Jebara, editors, Proceedings of the 31st International Conference on Machine Learning, volume 32 of Proceedings of Machine Learning Research, pages 665–673, 6 2014.
 - [53] S. Athey, J. Tibshirani, and S. Wager. Generalized random forests. Annals of Statistics, 47(2):

- 1148–1178, 2019.
- [54] Diederik P Kingma and Jimmy Ba. Adam: A method for stochastic optimization. [arXiv preprint arXiv:1412.6980](#), 2014.
 - [55] Charles J Stone. Consistent Nonparametric Regression. *Ann. Stat.*, 5(4):595–620, July 1977.
 - [56] Gido M van de Ven and Andreas S Tolias. Generative replay with feedback connections as a general strategy for continual learning. [arXiv preprint arXiv:1809.10635](#), 2018.
 - [57] James Martens. New insights and perspectives on the natural gradient method. [arXiv preprint arXiv:1412.1193](#), 2014.

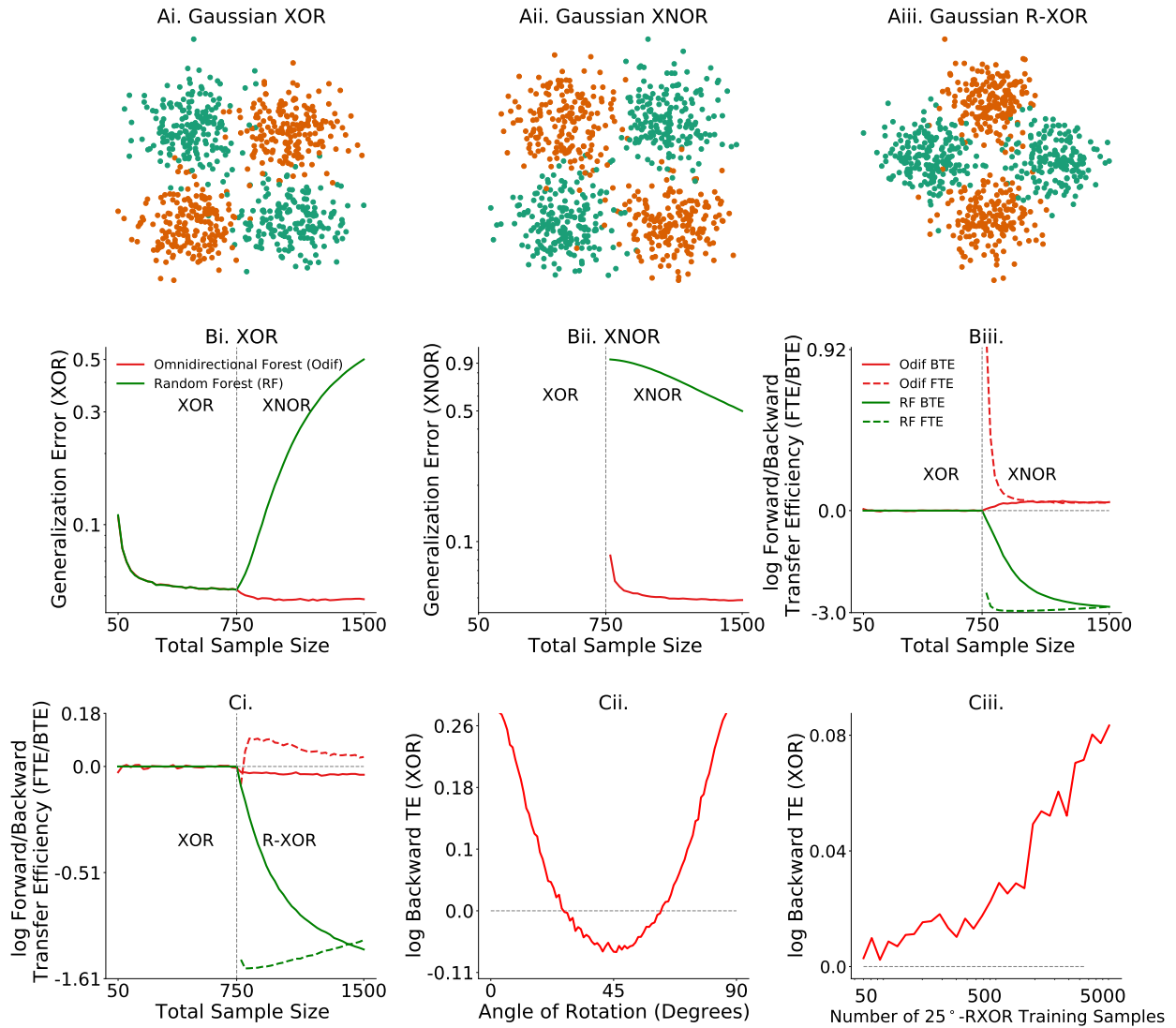


Figure 2: **Omnidirectional Forests demonstrate forward and backward transfer.** (A) 750 samples from: (Ai) Gaussian XOR, (Aii) XNOR, which has the same optimal discriminant boundary as XOR, and (Aiii) R-XOR, which has a discriminant boundary that is uninformative, and therefore adversarial, to XOR. (Bi) Generalization error for XOR, and (Bii) XNOR of both ODIF (red) and RF (green). ODIF outperforms RF on XOR when XNOR data is available, and on XNOR when XOR data are available. (Biii) Forward and backward transfer efficiency of ODIF are positive for all sample sizes, and are negative for all sample sizes for RF. (Ci) In an adversarial task setting (XOR followed by R-XOR), ODIF gracefully forgets XOR while positively forward transferring to R-XOR, whereas RF demonstrates catastrophic forgetting and interference. (Cii) log BTE with respect to XOR is positive when the optimal decision boundary of θ -XOR is similar to that of XOR (e.g. angles near 0° and 90°), and negative when the discriminant boundary is uninformative, and therefore adversarial, to XOR (e.g. angles near 45°). (Ciii) BTE increases monotonically with respect to sample size for XOR versus 25° -XOR.

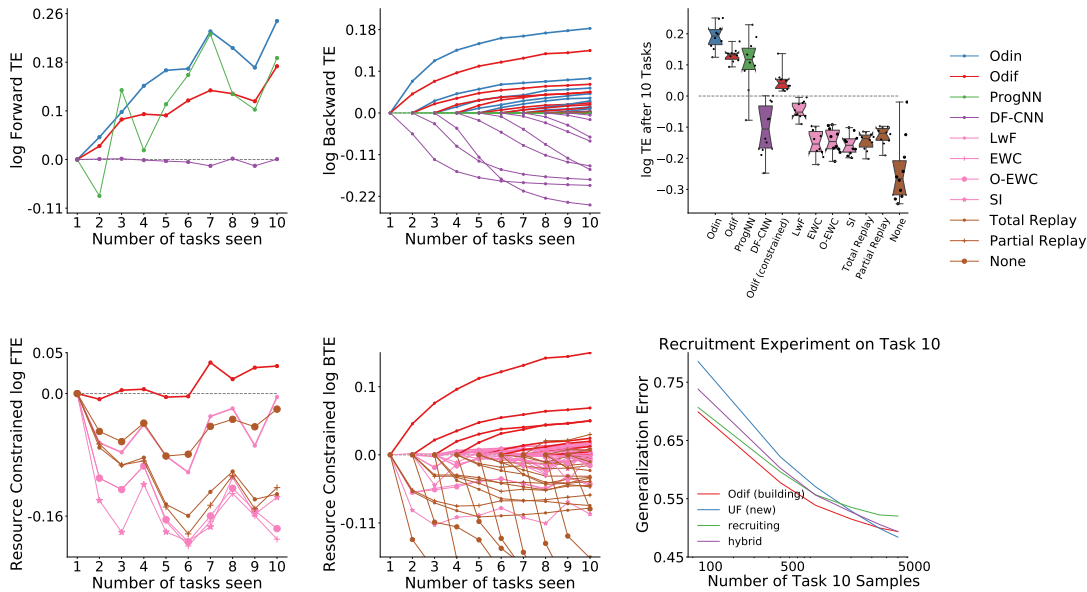


Figure 3: **Performance of different algorithms on the CIFAR 10x10 vision experiments.** *Top left and center:* Forward and backward transfer efficiency for various resource building algorithms. ODIF and ODIN consistently demonstrate both forward and backward transfer for each task, whereas ProgNN and DF-CNN do not. *Bottom left and center:* Same as above but comparing each algorithm with a fixed amount of resources. ODIF is the only approach that demonstrates forward or backward transfer. *Top right:* Transfer efficiencies of various algorithms for the 10 tasks after seeing the 10-th task. *Bottom right:* Building and recruiting ensembles are two boundaries of a continuum, with hybrid models in the middle. ODIF achieves lower (better) generalization error than other approaches until 5,000 training samples on the new task are available, but eventually a hybrid approach wins.

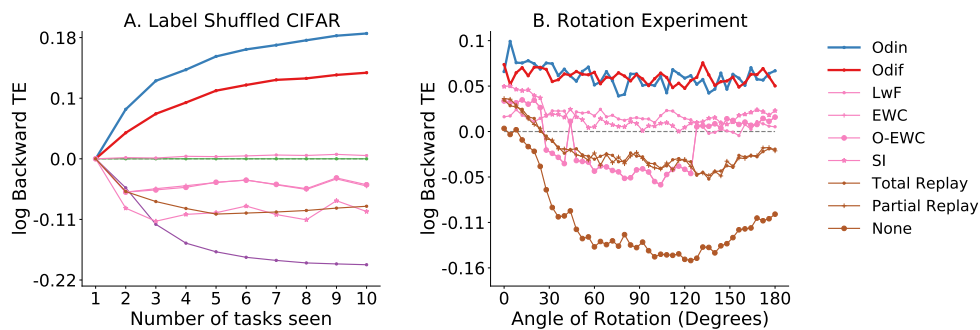


Figure 4: **Extended CIFAR 10x10 experiments.** (A) Shuffling class labels within tasks two through nine with 500 samples each demonstrates both ODIF and ODIN can still achieve positive backward transfer, and that the other algorithms still fail to transfer. (B) ODIF and ODIN are nearly invariant to rotations, whereas other approaches are more sensitive to rotation.

Appendix A. Decision Tree as a Compositional Hypothesis. Consider learning a decision tree for a two class classification problem. The input to the decision tree is a set of n feature-vector/response pairs, (x_i, y_i) . The learned tree structure corresponds to the representer u , because the tree structure maps each input feature vector into an indicator encoding in which leaf node each feature vector resides. Formally, $u : \mathcal{X} \mapsto [L]$, where $[L] = \{1, 2, \dots, L\}$ and L is the total number of leaf nodes. In other words, u maps from the original data space, to a L -dimensional one-hot encoded sparse binary vector, where the sole non-zero entry indicates in which leaf node a particular observation falls, that is, $\tilde{x} := u(x) \in \{0, 1\}^L$ where $\|\tilde{x}\| = 1$.

Learning the voter is simply a matter of counting the fraction of observations in each leaf per class. So, the voter is trained using n pairs of transformed feature-vector/response pairs (\tilde{x}_i, y_i) , and it assigns a probability of each class in each leaf: $\{v_l := \mathbb{P}[y_i = 1 | \tilde{x}_i = l], \forall l \in [L]\}$ and $v(\tilde{x}) = v_{\tilde{x}}$. In other words, for two class classification, v maps from the L -dimensional binary vector to the probability that x is in class 1. The decider is simply $w(v(\tilde{x})) = \mathbb{1}_{\{v(\tilde{x}) > 0.5\}}$, that is, it outputs the most likely class label of the leaf node that x falls into.

For inference, the tree is given a single x , and it is passed down the tree until it reaches a leaf node, where it is represented by its leaf identifier \tilde{x} . The voter takes \tilde{x} as input, and outputs the estimated posterior probability of being in class 1 for the leaf node in which \tilde{x} resides: $v(\tilde{x}) = \mathbb{P}[y = 1 | \tilde{x}]$. If $v(\tilde{x})$ is bigger than 0.5, the decider decides that x is in class 1, and otherwise, it decides it is in class 0.

Appendix B. Compositional Representation Ensembling. Consider a scenario in which we have two tasks, one following the other. Assume that we already learned a single decomposable hypothesis for the first task: $w_1 \circ v_1 \circ u_1$, and then we get new data associated with a second task. Let n_1 denote the sample size for the first task, and n_2 denote the sample size for the second task, and $n = n_1 + n_2$. The representation ensembling approach generally works as follows. First, since we want to transfer forward to the second task, we push all the new data through the first representer u_1 , which yields $\tilde{x}_{n_1+1}^{(1)}, \dots, \tilde{x}_n^{(1)}$. Second, we learn a new representer u_2 using the new data, $\{(x_i, y_i)\}_{i=n_1+1}^n$. We then push the new data through the new representer, yielding $\tilde{x}_{n_1+1}^{(2)}, \dots, \tilde{x}_n^{(2)}$. Third, we train a new omni-voter, v_2 . To do so, v_2 is trained on the outputs from both representers, that is, $\{(\tilde{x}_i^{(j)}, y_i)\}_{i=n_1+1}^n$ for $j = 1, 2$. The output of v_2 for any new input x is the posterior probability (or score) for that point for each potential response in task two (class label). Thus, by virtue of ensembling these representations, this approach enables forward transfer [16, 49].

Now, we would also like to improve performance on the first task using the second task’s data. While many lifelong methods have tried to achieve this kind of backward transfer, to date, they have mostly failed [15]. Recall that previously we had already pushed all the first task data through the first task representer, which had yielded $\tilde{x}_1^{(1)}, \dots, \tilde{x}_{n_1}^{(1)}$. Assuming we kept any of the first task’s data, or can adequately simulate it, we can push those data through u_2 to get a second representation of the first task’s data: $\tilde{x}_1^{(2)}, \dots, \tilde{x}_{n_1}^{(2)}$. Then, v_1 would be trained on both representations of the first task’s data. This ‘replay-like’ procedure facilitates backward transfer, that is, improving performance on previous tasks by leveraging data from newer tasks. Both the forward and backward transfer updates can be implemented every time we obtain data associated with a new task. **Enabling the omni-voters to ensemble omnidirectionally between all sets of tasks is the key innovation of our proposed omnidirectional learning approaches.**

Appendix C. Omnidirectional Algorithms. We propose two concrete omnidirectional algorithms, Omnidirectional Forests (ODIF) and Omnidirectional Networks (ODIN). The two algorithms differ in their

Algorithm 1 Add a new `ODIX` representer for a task. OOB = out-of-bag.

Input:

- (1) t ▷ current task number
- (2) $\mathcal{D}_n^t = (\mathbf{x}^t, \mathbf{y}^t) \in \mathbb{R}^{n \times p} \times \{1, \dots, K\}^n$ ▷ training data for task t

Output:

- (1) u_t ▷ a representer set
 - (2) \mathcal{I}_{OOB}^t ▷ a set of the indices of OOB data
 - 1: **function** `ODIX.FIT`($t, (\mathbf{x}^t, \mathbf{y}^t)$)
 - 2: $u_t, \mathcal{I}_{OOB}^t \leftarrow X.\text{fit}(\mathbf{x}^t, \mathbf{y}^t)$ ▷ train a representer X on bootstrapped data
 - 3: **return** u_t, \mathcal{I}_{OOB}^t
 - 4: **end function**
-

Algorithm 2 Add a new `ODIX` voter for the current task.

Input:

- (1) t ▷ current task number
- (2) $\mathbf{u}_t = \{u_{t'}\}_{t'=1}^t$ ▷ the set of representers
- (3) $\mathcal{D}_n^t = (\mathbf{x}^t, \mathbf{y}^t) \in \mathbb{R}^{n \times p} \times \{1, \dots, K\}^n$ ▷ training data for task t
- (4) \mathcal{I}_{OOB}^t ▷ a set of the indices of OOB data for the current task

Output: $\mathbf{v}_t = \{v_{t'}\}_{t'=1}^t$ ▷ in-task ($t' = t$) and cross-task ($t' \neq t$) voters for task t

- 1: **function** `ODIX.ADD_VOTER`($t, \mathbf{u}_t, (\mathbf{x}_t, \mathbf{y}_t), \mathcal{I}_{OOB}^t$)
 - 2: $v_{tt} \leftarrow u_t.\text{add_voter}((\mathbf{x}_t, \mathbf{y}_t), \mathcal{I}_{OOB}^t)$ ▷ add the in-task voter using OOB data
 - 3: **for** $t' = 1, \dots, t - 1$ **do** ▷ update the cross task voters for task t
 - 4: $v_{tt'} \leftarrow u_{t'}.\text{add_voter}(\mathbf{x}_t, \mathbf{y}_t)$
 - 5: **end for**
 - 6: **return** \mathbf{v}_t
 - 7: **end function**
-

details of how to update representers and voters, but abstracting a level up they are both special cases of the same procedure. Let `ODIX` refer to any possible omnidirectional algorithm. Algorithms 1, 2, 3, and 4 provide pseudocode for adding representers, updating voters, and making predictions for any `ODIX` algorithm; the below sections provide `ODIF` and `ODIN` specific details.

C.1 Omnidirectional Forests A Omnidirectional Forest (`ODIF`) is a decision forest-based instance of ensembling representations. For each task, the transformer u_t of a `ODIF` is a decision forest [37, 50]. The leaf nodes of each decision tree partition the input space \mathcal{X} [51]. The representation of $x \in \mathcal{X}$ corresponding to a single tree can be a one-hot encoded L_b -dimensional vector with a 1 in the location corresponding to the leaf x falls into of tree b . The representation of x resulting from the collection of trees simply concatenates the B one-hot vectors from the B trees. Thus, the the transformer u_t is the mapping from \mathcal{X} to a B -sparse vector of length $\sum_{b=1}^B L_b$. The posteriors are learned by populating the cells of the partitions and taking class votes with out-of-bag samples, as in ‘honest trees’ [51–53]. The posteriors output the average normalized class votes across the collection of trees, adjusted for finite sample bias [38]. The decider w_t averages the posterior estimates and outputs the argmax to produce a single prediction. Recall that honest decision forests are universally consistent classifiers and regressors [53], meaning that with sufficiently large sample sizes, under suitable though general assumptions, they will converge to minimize risk. The single task version of this approaches simplifies

Algorithm 3 Update ODI_X voter for the previous tasks.

Input:

- (1) t ▷ current task number
- (2) u_t ▷ representer for the current task
- (3) $\mathcal{D} = \{\mathcal{D}^{t'}\}_{t'=1}^{t-1}$ ▷ training data for tasks $t' = 1, \dots, t-1$

Output: $v = \{v_{t'}\}_{t'=1}^{t-1}$ ▷ all previous task voters

```
1: function ODIX.UPDATE_VOTER( $t, u_t, \mathcal{D}$ )
2:   for  $t' = 1, \dots, t-1$  do ▷ update the cross task voters
3:      $v_{t't} \leftarrow u_t.\text{get\_voter}(\mathbf{x}_{t'}, \mathbf{y}_{t'})$ 
4:   end for
5:   return  $v$ 
6: end function
```

Algorithm 4 Predicting a class label using ODI_X.

Input:

- (1) $x \in \mathbb{R}^p$ ▷ test datum
- (2) t ▷ task identity associated with x
- (3) \mathbf{u} ▷ all T representers
- (4) v_t ▷ voter for task t

Output: \hat{y} ▷ a predicted class label

```
1: function  $\hat{y} = \text{ODI}_X.\text{PREDICT}(t, x, v_t)$ 
2:    $T \leftarrow \text{ODI}_X.\text{get\_task\_number}()$  ▷ get the total number of tasks
3:    $\hat{\mathbf{p}}_t = \mathbf{0}$  ▷  $\hat{\mathbf{p}}_t$  is a  $K$ -dimensional posterior vector
4:   for  $t' = 1, \dots, T$  do ▷ update the posteriors calculated from  $T$  task voters
5:      $\hat{\mathbf{p}}_t \leftarrow \hat{\mathbf{p}}_t + v_{tt'}.\text{predict\_proba}(u_{t'}(x))$ 
6:   end for
7:    $\hat{\mathbf{p}}_t \leftarrow \hat{\mathbf{p}}_t / T$ 
8:    $\hat{y} = \text{argmax}_i(\hat{\mathbf{p}}_t)$  ▷ find the index  $i$  of the elements in the vector  $\hat{\mathbf{p}}_t$  with maximum probability
9:   return  $\hat{y}$ 
10: end function
```

to an approach called ‘Uncertainty Forests’ [38]. Table 1 lists the hyperparameters used in the CIFAR experiments.

Table 1: Hyperparameters for ODI_F in CIFAR experiments. n_estimators is denoted by B , the number of trees, above.

Hyperparameters	Value
n_estimators (500 training samples per task)	10
n_estimators (5000 training samples per task)	40
max_depth	30
max_samples	0.67
min_samples_leaf	1

C.2 Omnidirectional Networks An Omnidirectional Network (ODIN) is a deep network (DN) based instance of ensembling representations. For each task, the representer u_t in an ODIN is the “backbone”

of a DN, including all but the final layer. Thus, each u_t maps an element of \mathcal{X} to an element of \mathbb{R}^d , where d is the number of neurons in the penultimate layer of the DN. In practice, we use the architecture described in van de Ven et al. [25] as “5 convolutional layers followed by 2 fully-connected layers each containing 2,000 nodes with ReLU non-linearities and a softmax output layer.” We trained this network using cross-entropy loss and the Adam optimizer [54] to learn the transformer. The omni-voters are learned via k -Nearest Neighbors (k -NN) [55]. Recall that a k -NN, with k chosen such that as the number of samples n goes to infinity k goes to infinity and $\frac{k}{n} \rightarrow 0$, is a universally consistent classifier [55]. We use $k = 16 \log_2 n$, which satisfies these conditions.

C.3 Reference Algorithm Implementation Details The same network architecture was used for all compared deep learning methods. Following van de Ven et al. [25], the ‘base network architecture’ consisted of five convolutional layers followed by two-fully connected layers each containing 2000 nodes with ReLU non-linearities and a softmax output layer. The convolutional layers had 16, 32, 64, 128 and 254 channels, they used batch-norm and a ReLU non-linearity, they had a 3x3 kernel, a padding of 1 and a stride of 2 (except the first layer, which had a stride of 1). This architecture was used with a multi-headed output layer (i.e., a different output layer for each task) for all algorithms using a fixed-size network. For ProgNN and DF-CNN the same architecture was used for each column introduced for each new task, and in our ODIN this architecture was used for the transformers u_t (see above). In these implementations, ProgNN and DF-CNN have the same architecture for each column introduced for each task. Each column has an input layer followed by 4 convolutional layer with size $3 \times 3 \times 32$, $3 \times 3 \times 32$, $3 \times 3 \times 64$ and $3 \times 3 \times 64$, respectively. It is followed by a fully-connected layer with 64 nodes and an output layer with 10 nodes. ReLU activation was used after each layer. The other algorithms use a common architecture with input layers defined by the size of the input data, two hidden layers with 400 nodes each and a multi-headed output layer (different output layers for different tasks). Different algorithms only differ in the way they penalize the update of network parameters for the current task based on the previous tasks. Each of these algorithms has 1.4M parameters in total. Below we provide a brief description of the architecture and regularization terms used by these algorithms.

ProgNN ProgNN can be explained in a simple manner using a two task environment. For the first task, it trains a single column with L layers having the hidden activations $h_i^{(1)} \in \mathbb{R}^{n_i}$, where n_i is the number of units at layer $i \leq L$ and $\theta^{(1)}$ represents the parameters to be learned for task one. Once the $\theta^{(1)}$ is learned, a new column with parameters $\theta^{(2)}$ is added to the architecture for the second task where layer $h_i^{(2)}$ receives input from both from the previous layer in the same column $h_{i-1}^{(1)}$ and the column for the first task $h_{i-1}^{(2)}$. This can be generalized for k -th task and i -th layer as

$$(1) \quad h_i^{(k)} = f \left(\mathbf{W}_i^{(k)} h_{i-1}^{(k)} + \sum_{j < k} \mathbf{U}_i^{(k:j)} h_{i-1}^{(j)} \right),$$

where $\mathbf{W}_i^{(k)} \in \mathbb{R}^{n_i \times n_{i-1}}$ is the weight matrix of layer i of column k , $\mathbf{U}_i^{(k:j)} \in \mathbb{R}^{n_i \times n_j}$ are the lateral connections from layer $i - 1$ of column j , to layer i of column k , f is an element-wise non-linearity and h_0 is the network input. This architecture enables forward transfer of learning between tasks while providing no scope for backward transfer. It has 3.51M parameters in total.

DF-CNN DF-CNN introduces a new convolutional neural network CNN_t for each new task t in the architecture. For each convolutional layer $l \in 1, \dots, d$ of each CNN_t , $\mathbf{W}_t^{(l)} \in \mathbb{R}^{h \times w \times c_{in} \times c_{out}}$ is the corresponding filter with height h , width w , input channels c_{in} and output channels c_{out} . These filters

are adapted from a task-independent layer-dependent knowledge base $L^{(l)}$ for each layer l that is shared among all the tasks. The filters $\mathbf{W}_t^{(l)}$ are generated from learned latent knowledge base $L^{(l)}$ by the deconvolution operator, followed by a tensor contraction. The implementation for DF-CNN has 7.96M parameters in total.

EWC In EWC, the update of parameters θ is regularized so that the parameters that are more important for the previous tasks are not allowed to change much and the comparatively less important parameters are allowed to model the new task. The relative importance of different parameters for each task is measured using the corresponding diagonal element of that task’s Fisher information matrix, evaluated at the optimal parameter values after finishing training on that task. The EWC regularization term for task $K > 1$ is given by:

$$(2) \quad \mathcal{L}_{regularization_{EWC}}^{(K)}(\theta) = \sum_{k=1}^{K-1} \left(\frac{1}{2} \sum_{i=1}^{N_{params}} F_{ii}^{(k)} (\theta_i - \hat{\theta}_i^{(k)})^2 \right)$$

where $\hat{\theta}_i^{(k)}$ is the i -th element of $\hat{\theta}^{(k)}$. $\hat{\theta}^{(k)}$ is the vector of optimum parameter values after training for task k . Here $F_{ii}^{(k)}$ is the i -th diagonal element of empirical Fisher information matrix, $\mathbf{F}^{(k)}$, defined in [56], [57].

Online EWC The main disadvantage of EWC is the regularization term grows in size with the number of tasks. To overcome this problem, Online EWC uses the following regularization term while training on task $k > 1$:

$$(3) \quad \mathcal{L}_{regularization_{oEWC}}^{(K)}(\theta) = \sum_{i=1}^{N_{params}} \tilde{F}_{ii}^{(k-1)} (\theta_i - \hat{\theta}_i^{(k-1)})^2$$

where $\hat{\theta}_i^{(k-1)}$ is the value of parameter i after finishing on task $k - 1$. $\tilde{F}_{ii}^{(k-1)}$ is estimated in an iterative way as

$$(4) \quad \tilde{F}_{ii}^{(k-1)} = \gamma \tilde{F}_{ii}^{(k-2)} + F_{ii}^{(k-1)}$$

where $\gamma \leq 1$ is a hyperparameter that governs the decay of contribution from the previous tasks and $\tilde{F}_{ii}^{(1)} = F_{ii}^{(1)}$ and $F_{ii}^{(k)}$ is the i -th diagonal element of the empirical Fisher information matrix for k -th task described earlier.

SI Like EWC and Online EWC, SI also uses a quadratic regularization term, with the weight of each parameter’s penalty depending on the importance of that parameter for the tasks learned so far. However, instead of using Fisher information matrix, a per-parameter contribution to the loss is calculated for each parameter i as

$$(5) \quad \omega_i^{(k)} = \sum_{t=1}^{N_{iters}} \left(\theta_i[t^{(k)}] - \theta_i[(t-1)^{(k)}] \right) \frac{\delta \mathcal{L}_{total}[t^{(k)}]}{\delta \theta_i}$$

where N_{iters} is the total number of iterations per task, $\theta_i[t^{(k)}]$ is the value of i -th parameter at t -th training iteration on task k and $\frac{\delta \mathcal{L}_{total}[t^{(k)}]}{\delta \theta_i}$ is the gradient of the total loss function with respect to θ_i at

t -th iteration of task k . Now the estimated importance of parameter i for the first $K - 1$ tasks is given by:

$$(6) \quad \Omega_i^{(K-1)} = \sum_{k=1}^{K-1} \frac{\omega_i^{(k)}}{\left(\Delta_i^{(k)}\right)^2 + \xi}$$

where $\Delta_i^{(k)} = \theta_i[N_{iters}^{(k)}] - \theta_i[0^{(k)}]$. $\theta_i[0^{(k)}]$ is the initialized value of the parameter i . Finally, the regularization term for SI is given by:

$$(7) \quad \mathcal{L}_{regularization_{SI}}^{(K)}(\theta) = \sum_{i=1}^{N_{params}} \Omega_i^{(K-1)} (\theta_i - \hat{\theta}_i^{(K-1)})^2$$

LwF For LwF, the total loss function \mathcal{L}_{total} consists of two parts:

$$(8) \quad \mathcal{L}_{total} = \frac{1}{N_{tasks \text{ so far}}} \mathcal{L}_{current} + \left(1 - \frac{1}{N_{tasks \text{ so far}}}\right) \mathcal{L}_{replay}$$

Here $\mathcal{L}_{current}$ includes the original input data-label pairs for the current task. However, for the \mathcal{L}_{replay} part, pseudo labels are assigned to the input data for the current task predicted using the model trained on the data up to the previous task.

Appendix D. Simulated Results. In each simulation, we constructed an environment with two tasks. For each, we sample 750 times from the first task, followed by 750 times from the second task. These 1,500 samples comprise the training data. We sample another 1,000 hold out samples to evaluate the algorithms. We fit a random forest (RF) (technically, an uncertainty forest which is an honest forest with a finite-sample correction [38]) and a ODIF. We repeat this process 30 times to obtain errorbars. Errorbars in all cases were negligible.

D.1 Gaussian XOR Gaussian XOR is two class classification problem with equal class priors. Conditioned on being in class 0, a sample is drawn from a mixture of two Gaussians with means $\pm [0.5, 0.5]^T$, and variances proportional to the identity matrix. Conditioned on being in class 1, a sample is drawn from a mixture of two Gaussians with means $\pm [0.5, -0.5]^T$, and variances proportional to the identity matrix. Gaussian XNOR is the same distribution as Gaussian XOR with the class labels flipped. Rotated XOR (R-XOR) rotates XOR by θ° degrees.

D.2 Spirals A description of the distributions for the two tasks is as follows: let K be the number of classes and $S \sim \text{multinomial}(\frac{1}{K} \mathbf{1}_K, n)$. Conditioned on S , each feature vector is parameterized by two variables, the radius r and an angle θ . For each sample, r is sampled uniformly in $[0, 1]$. Conditioned on a particular class, the angles are evenly spaced between $\frac{4\pi(k-1)t_K}{K}$ and $\frac{4\pi(k)t_K}{K}$ where t_K controls the number of turns in the spiral. To inject noise along the spiral, we add Gaussian noise to the evenly spaced angles $\theta' : \theta = \theta' + \mathcal{N}(0, \sigma_K^2)$. The observed feature vector is then $(r \cos(\theta), r \sin(\theta))$. In Figure 1 we set $t_3 = 2.5$, $t_5 = 3.5$, $\sigma_3^2 = 3$ and $\sigma_5^2 = 1.876$.

Consider an environment with a three spiral and five spiral task (Figure 1). In this environment, axis-aligned splits are inefficient, because the optimal partitions are better approximated by irregular polytopes than by the orthotopes provided by axis-aligned splits. The three spiral data helps the five spiral performance because the optimal partitioning for these two tasks is relatively similar to one

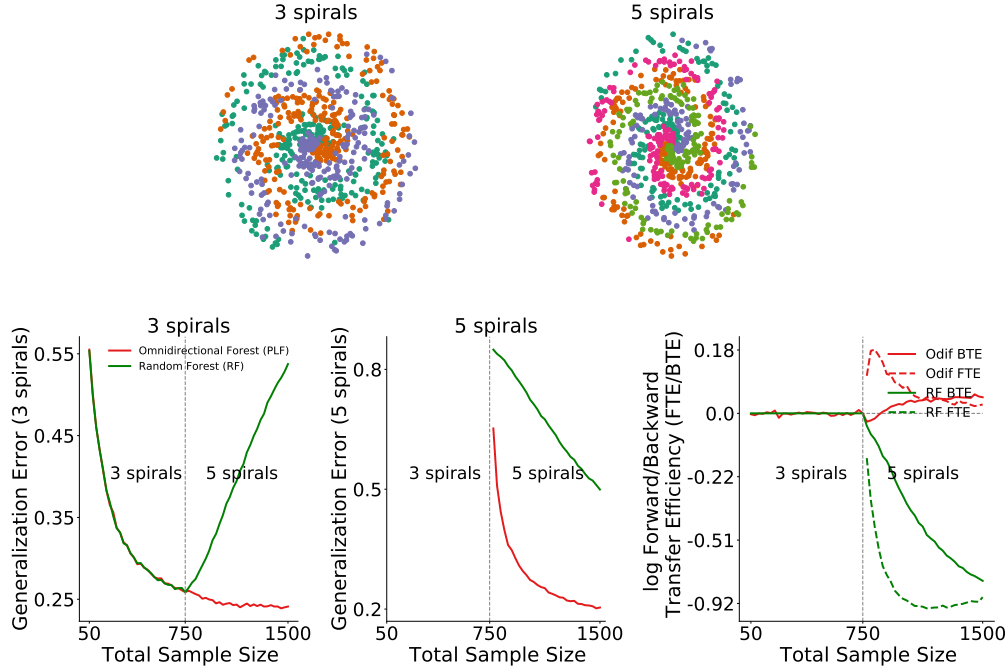


Figure 1: *Top*: 750 samples from 3 spirals (left) and 5 spirals (right). *Bottom left*: ODIF outperforms RF on 3 spirals when 5 spirals data is available, demonstrating *backward* transfer in ODIF . *Bottom center*: ODIF outperforms RF on 5 spirals when 3 spirals data is available, demonstrating *forward* transfer in ODIF . *Bottom right*: Transfer Efficiency of ODIF . The forward (solid) and backward (dashed) curves are the ratio of the generalization error of ODIF to RF in their respective figures. ODIF demonstrates decreasing forward transfer and increasing backward transfer in this environment.

another, as indicated by positive forward transfer. This is despite the fact that the five spiral task requires more fine partitioning than the three spiral task. Because ODIF grows relatively deep trees, it over-partitions space, thereby rendering tasks with more coarse optimal decision boundaries useful for tasks with more fine optimal decision boundaries. The five spiral data also improves the three spiral performance.

Appendix E. Real Data Extended Results.

Table 2: Hyperparameters for ODIF in spoken digit experiment.

Hyperparameters	Value
n_estimators (275 training samples per task)	10
max_depth	30
max_samples	0.67
min_samples_leaf	1

E.1 Spoken Digit Experiment In this experiment, we used the spoken digit dataset provided in <https://github.com/Jakobovski/free-spoken-digit-dataset>. The dataset contains audio recordings from 6 different speakers with 50 recordings for each digit per speaker (3000 recordings in total). The experiment was set up with 6 tasks where each task contains recordings from only one speaker. For each recording, a spectrogram was extracted using Hanning windows of duration 16 ms with an overlap of 4 ms between the adjacent windows. The spectrograms were resized down to 28×28 . The extracted

Short-Time Fourier Transform Spectrogram of Number 5

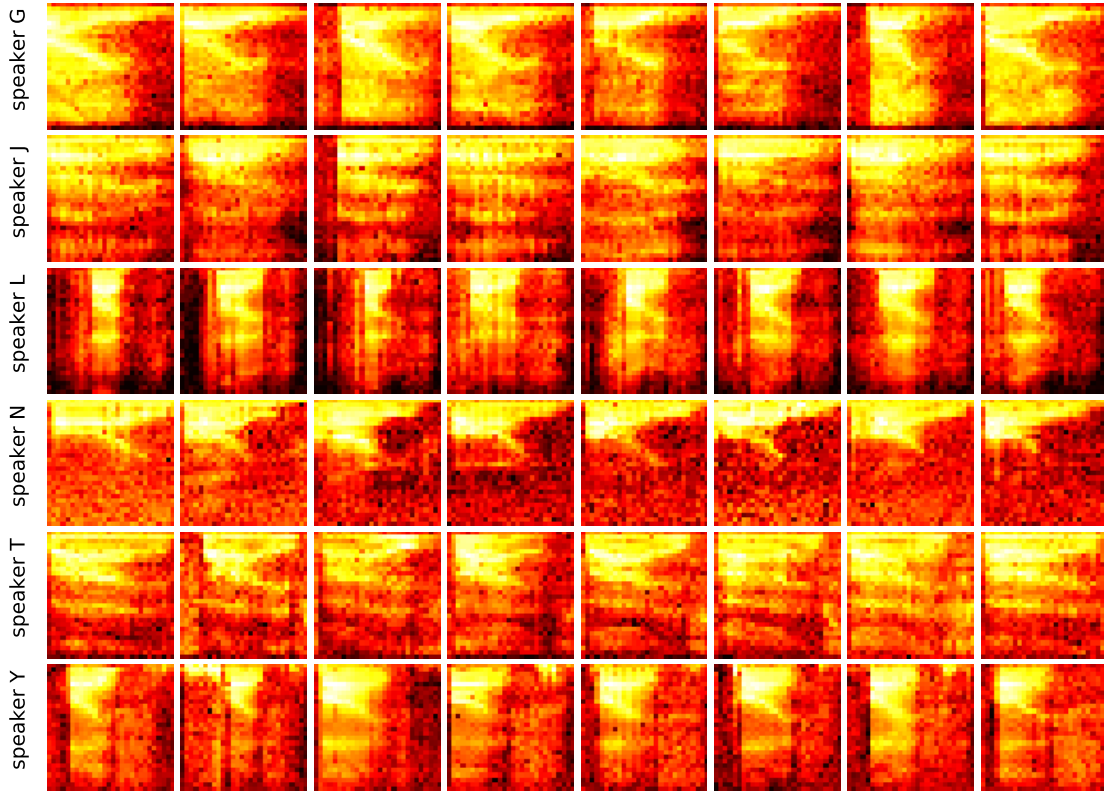


Figure 2: Spectrogram extracted from 8 different recordings of 6 speakers uttering the digit ‘5’.

spectrograms from 8 random recordings of ‘5’ for 6 speakers are shown in Figure 2. For each Monte Carlo repetition of the experiment, spectrograms extracted for each task were randomly divided into 55% train and 45% test set. As shown in Figure 3, both $ODIF$ and $ODIN$ show positive transfer between the spoken digit tasks.

E.2 CIFAR 10x10 Supplementary Table 3 shows the image classes associated with each task number. Supplementary Figure 4 is the same as Figure 3 but with 5,000 training samples per task, rather than 500. Notably, with 5,000 samples, replay methods are able to transfer both forward and backward as well, though recall they are considerably more computationally intensive than $ODIN$ and $ODIF$.

E.3 CIFAR Label Shuffling Supplementary Figure 5 shows the same result as the label shuffling from Figure 4, but with 5,000 samples per class. The results for $ODIN$ and $ODIF$ are qualitatively similar, in that they transfer backwards. The replay methods are also able to transfer when using this larger number of samples, although with considerably higher computational cost.

E.4 CIFAR 10x10 Repeated Classes We also considered the setting where each task is defined by a random sampling of 10 out of 100 classes with replacement. This environment is designed to demonstrate the effect of tasks with shared subtasks, which is a common property of real world lifelong

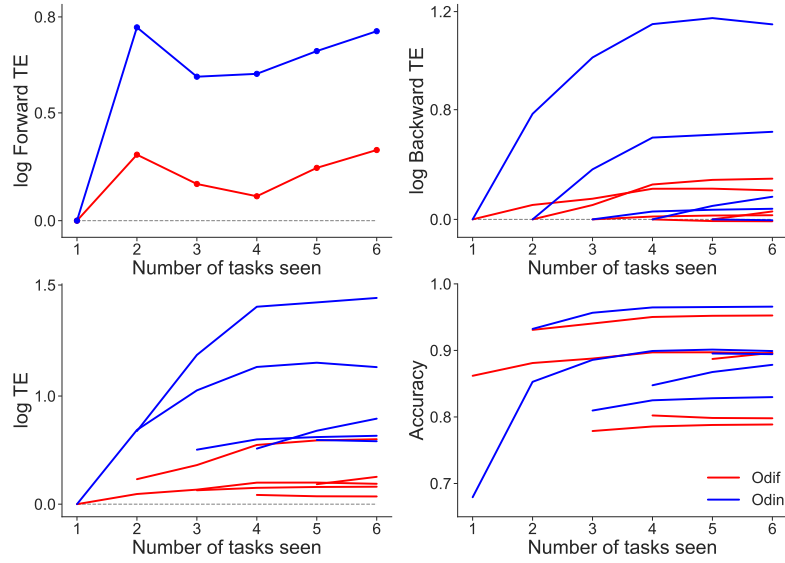


Figure 3: Both ODIF and ODIN shows positive forward and backward transfer for the spoken digit tasks.

Table 3: Task splits for CIFAR 10x10.

Task #	Image Classes
1	apple, aquarium fish, baby, bear, beaver, bed, bee, beetle, bicycle, bottle
2	bowl, boy, bridge, bus, butterfly, camel, can, castle, caterpillar
3	chair, chimpanzee, clock, cloud, cockroach, couch, crab, crocodile, cup, dinosaur
4	dolphin, elephant, flatfish, forest, fox, girl, hamster, house, kangaroo, keyboard
5	lamp, lawn mower, leopard, lion, lizard, lobster, man, maple tree, motor cycle, mountain
6	mouse, mushroom, oak tree, orange, orchid, otter, palm tree, pear, pickup truck, pine tree
7	plain, plate, poppy, porcupine, possum, rabbit, raccoon, ray, road, rocket
8	rose, sea, seal, shark, shrew, skunk, skyscraper, snail, snake, spider
9	squirrel, streetcar, sunflower, sweet pepper, table, tank, telephone, television, tiger, tractor
10	train, trout, tulip, turtle, wardrobe, whale, willow tree, wolf, woman, worm

learning tasks. Supplementary Figure 6 shows transfer efficiency of ODIF and ODIN on Task 1.

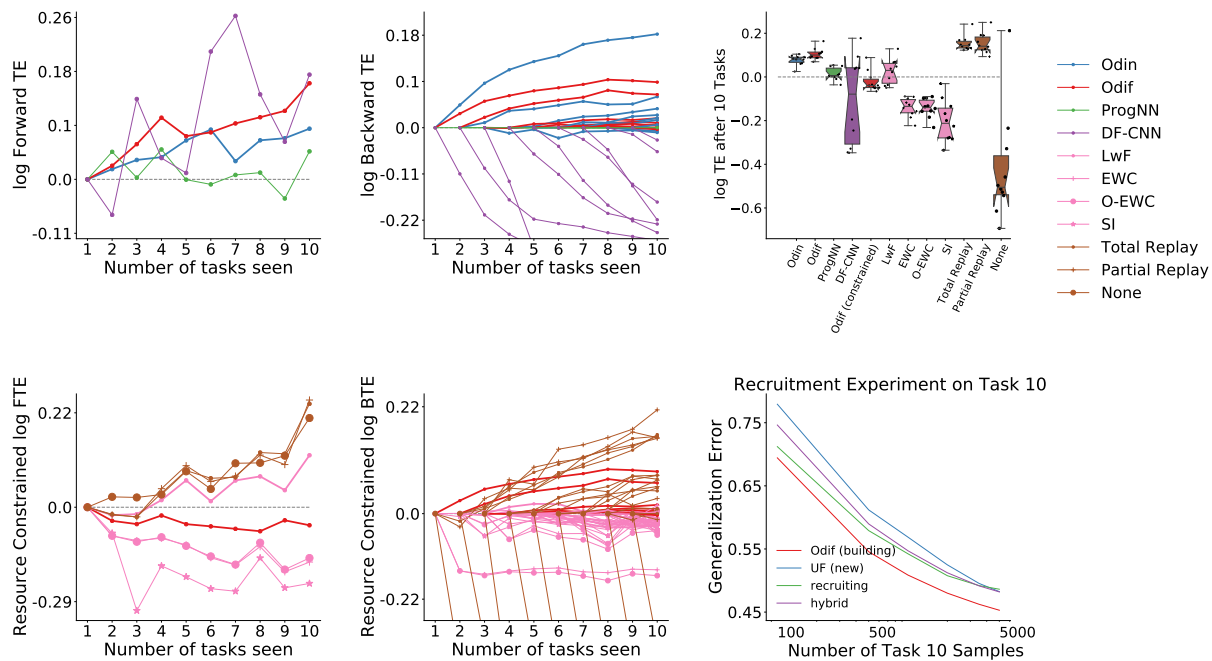


Figure 4: Performance of different algorithms on CIFAR 10x10 vision dataset for 5,000 training samples per task. ODIN maintains approximately the same forward transfer (top left and bottom left) and backward transfer (top center and bottom center) efficiency as those for 500 samples per task whereas other algorithms show reduced or nearly unchanged transfer. ODIF still demonstrates positive forward, backward, and final transfer, unlike most of the state-of-the-art algorithms, which demonstrate forgetting. The replay methods, however, do demonstrate transfer, albeit with significantly higher computational cost.

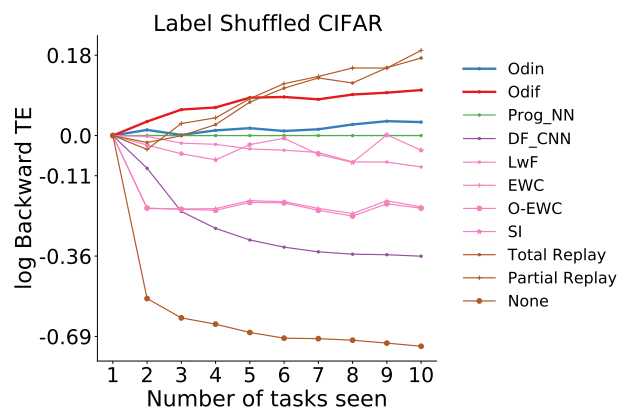


Figure 5: **Label shuffle experiment on CIFAR 10x10 vision dataset for 5,000 training samples per task.** Shuffling class labels within tasks two through nine with 5000 samples each demonstrates both ODIF and ODIN can still achieve positive backward transfer, and that the other algorithms that do not replay the previous task data fail to transfer.

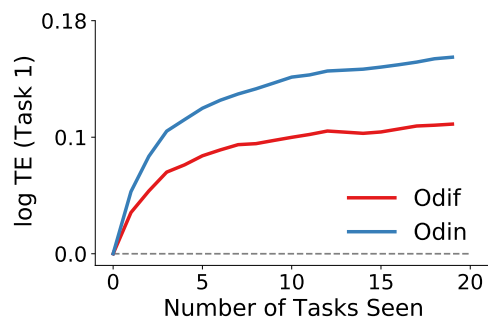


Figure 6: ODIF and ODIN transfer knowledge effectively when tasks share common classes. Each task is a random selection of 10 out of the 100 CIFAR-100 classes. Both ODIF and ODIN demonstrate monotonically increasing transfer efficiency for up to 30 tasks.